

1
2
3
4
5
6
7
8
9
10
11
12
13 **Enhancing irreversible electroporation by manipulating cellular biophysics with a**
14 **molecular adjuvant**
15
16 JW Ivey, EL Latouche, ML Richards, GJ Lesser, W Debinski, RV Davalos, SS Verbridge
17
18 Running Title: Cell morphology and electroporation
19
20

21 **Abstract**

22 Pulsed electric fields (PEFs) applied to cells have been used as an invaluable research tool to
23 enhance delivery of genes or other intracellular cargo, as well as for tumor treatment via
24 electrochemotherapy or tissue ablation. These processes involve the buildup of charge across the
25 cell membrane, with subsequent alteration of transmembrane potential that is a function of cell
26 biophysics and geometry. For traditional electroporation parameters, larger cells experience a
27 greater degree of membrane potential alteration. However, we have recently demonstrated that
28 nuclear-to-cytoplasm ratio (NCR), rather than cell size, is a key predictor of response for cells
29 treated with high-frequency irreversible electroporation (H-FIRE). In this study we leverage a
30 targeted molecular therapy, ephrinA1, known to markedly collapse the cytoplasm of cells
31 expressing the EphA2 receptor, to investigate how biophysical cellular changes resulting from
32 NCR manipulation affect response to irreversible electroporation (IRE) at varying frequencies.
33 We present evidence that the increase in NCR mitigates the cell death response to conventional
34 electroporation pulsed-electric fields ($\sim 100 \mu\text{s}$), consistent with the previously noted size
35 dependence. However this same molecular treatment enhanced cell death response to high
36 frequency electric fields ($\sim 1 \mu\text{s}$). This finding demonstrates the importance of considering
37 cellular biophysics and frequency-dependent effects in developing electroporation protocols,
38 while our approach provides a novel and direct experimental methodology to quantify the
39 relationship between cell morphology, pulse frequency and electroporation response. Finally,
40 this novel combinatorial approach may provide a paradigm to enhance *in vivo* tumor ablation
41 through a molecular manipulation of cellular morphology prior to IRE application.

42

43

44 **Introduction**

45 Electroporation describes the phenomenon of using an electric field to permeabilize the
46 membrane of a cell by inducing a transmembrane potential large enough to induce a disruption in
47 the lipid bilayer. Once the transmembrane potential reaches a critical value of ~ 250 mV,
48 transient nanoscale pores form in the membrane allowing the passage of otherwise excluded
49 molecules through the membrane barrier (1). This reversible electroporation technique has been
50 used for gene transfection, gene therapy, and cancer electrochemotherapy (ECT) (2, 3). When the
51 transmembrane potential reaches another critical value of ~ 1 V, the cell cannot recover from the
52 pore formation and dies due to loss of homeostasis (4). This method of cell ablation, termed
53 irreversible electroporation (IRE), has been used for the treatment of a variety of cancers
54 including prostate, pancreas, and liver cancers (5-8).

55

56 IRE as a cancer treatment method has many advantages over other approaches. The non-thermal
57 nature of the treatment allows for the sparing of extracellular matrix and vital structures such as
58 blood vessels while producing a more uniform ablation due to the lack of a heat sink effect (9).
59 IRE ablation methods are able to achieve cell-scale (~ 50 μ m) resolution between ablated and
60 non-ablated zones (9, 10) allowing for ablation regions to be predicted by pre-treatment planning
61 (11). In addition, real-time monitoring by imaging and impedance measurements can be done to
62 ensure proper electrode placement and complete ablation (12, 13). While the benefits of this
63 treatment modality have underpinned its successful use for a variety of cancers, invasive cancers
64 such as glioblastoma (GBM) still present challenges. IRE methods do not allow for the treatment
65 of diffuse cells outside the tumor margin without ablation of healthy tissue, a situation especially
66 problematic in the brain. To address these challenges and improve selectivity outside the tumor

67 margin, investigators have begun studying combination therapies such as IRE used with ECT
68 (14).

69

70

71 In order to increase the selective capabilities of IRE treatment, here we investigate a new
72 combinatorial treatment concept, combining electroporation with a molecular therapy that we
73 hypothesized would act in a synergistic manner to the physical treatment. Our previous research
74 efforts have identified the receptor EphA2 as a promising target for selective molecular treatment
75 for GBM (15). EphA2, a member of the largest class of receptor tyrosine kinases, is
76 overexpressed in GBM tissue in a predominantly inactive state (15) as its preferred ligand
77 ephrinA1 (eA1) is present at diminished levels compared to normal brain tissue (16, 17). Our
78 research efforts have shown that exogenous soluble eA1 is a functional ligand for EphA2 (18)
79 and progress has been made in creating ephrin-based therapeutic agents through conjugation of a
80 bacterial toxic protein to soluble eA1 that selectively targets GBM cells (19). From this work
81 developing an ephrin-based molecular targeted therapy, we noted a selective morphology change
82 in GBM cells upon exposure to eA1. This physical response, characterized by a rounding of the
83 cell and a shrinking of the cell cytoplasm (18, 20, 21), formed the basis of the currently presented
84 investigation into a combinatorial treatment with IRE therapies.

85

86 In considering IRE, the physical attributes of a cell are important, as electroporation is dependent
87 on both cell size and morphology. The effect of cell size on electroporation has been
88 demonstrated for a variety of pulse widths ranging from a few microseconds (22) to hundreds of
89 milliseconds (23). The steady-state scenario (Fig S1a) is valid for the understanding of

90 electroporation phenomenon involved in typical IRE protocols used in the treatment of cancer.
91 These protocols involve the application of around 90 pulses of 50-100 μ s duration delivered
92 through electrodes inserted into the tissue (5, 24). We have shown that by reducing the duration
93 of the electric field pulses to be shorter than the charging time of the cell membrane, the field can
94 penetrate the cell interior, and the dependence of electroporation on cell size is reduced (25, 26)
95 (Fig S1b). This shorter pulse technique, termed high-frequency IRE (H-FIRE), which uses trains
96 of $\leq 2\mu$ s duration bipolar pulses, exposes inner organelles to large electric fields. H-FIRE acts on
97 cells in a way that nuclear size becomes a more important predictor of cell death than cell size,
98 with a lower electric field needed to kill cells with a higher nuclear to cytoplasm ratio (NCR)
99 (25).

100
101 Despite some efforts to predict the TMP of cells exposed to PEFs on the order of a few
102 microseconds no mathematical models for cells of a high NCR have been developed (27) (28). In
103 this study we look further into the impact of cell size and morphology on electroporation
104 phenomenon at short pulse lengths, where the steady-state electroporation equation breaks down
105 and frequency is known to play an important role in predicting induced TMP. Equipped with the
106 finding that NCR is an important predictor of electroporation using H-FIRE pulse lengths, we
107 investigated the NCR effect on H-FIRE ablation by combining H-FIRE therapy with a molecular
108 intervention using eA1 to increase NCR.

109
110 The overabundance of EphA2 receptor and diminished presence of eA1 in GBM tissue open up
111 this receptor ligand interaction as a unique method for selectively tuning cell morphology to isolate
112 the NCR effect on H-FIRE. These biological cell manipulations allow us to discover

113 electroporation behaviors in the pulse space where traditional analytical model predictions do not
114 apply. Additionally, this work highlights a novel correlation—an increase in electroporation
115 efficacy due to decreasing cell size—thereby highlighting the complexities ignored by the Schwan
116 equation in describing cell response to electric fields with short pulses.

117

118 **Materials and Methods**

119 **Cell culture**

120 U-87 MG primary human glioblastoma cells (ATCC) were cultured in Dulbecco's Modified Eagle
121 Medium (DMEM) containing 10% fetal bovine serum (FBS) and 1% penicillin/streptomycin (PS).
122 Normal Human Astrocyte (NHA) cells (Lonza) were cultured in Astrocyte Growth Media (Lonza).
123 U-251 MG primary human glioblastoma cells (ATCC) cells were grown in DMEM containing
124 10% FBS, 1% PS, and 0.1 mM non-essential amino acid. DBTRG human glioblastoma cells
125 (ATCC) were culture in RPMI medium containing 10% FBS, 2 mM L-glutamine, 1% PS and
126 0.1 mM non-essential amino acids. All cells were grown in culture at 37 °C in 5% CO₂ in a
127 humidified incubator. Cells were seeded in hydrogels at a density of 1 × 10⁶ cells/mL. The
128 hydrogels were submerged in appropriate growth media for the cell type at 37 °C in 5% CO₂ in a
129 humidified incubator and cell viability was maintained within hydrogels for up to 7 days.

130 **Construction of collagen scaffolds**

131 Stocks of type I collagen were prepared by dissolving rat tail tendon in acetic acid, followed by
132 freezing and lyophilization as described previously (29). Stock solution concentrations of collagen
133 were created at a density of 10 mg/mL. Scaffolds with a final concentration of 5 mg/mL were made
134 from concentrated collagen stocks to create collagen gels of 0.5% (w/w). Neutralized collagen
135 solutions were created by mixing acid-dissolved collagen with 10X DMEM (10% of total collagen

136 solution volume) and sufficient volumes of 1N NaOH until a pH in the range of 7.0–7.4 was
137 achieved. The neutralized collagen was mixed with cells suspended in DMEM or NHA media to
138 achieve a cell density of 1×10^6 cells/mL in the final collagen mixture. Solutions were mixed
139 carefully with a sterilized spatula to ensure homogenous distribution throughout the gel without
140 damaging cells. Collagen solutions were then dispensed into a polydimethylsiloxane (PDMS)
141 mold with a cut-out of 10 mm diameter and 1 mm depth and molded flat to ensure consistent
142 scaffold geometry. Our previous mathematical modeling and experiments on oxygen (O_2)
143 consumption rates by tumor cells(29) confirms that at this cell density and scaffold thickness, O_2
144 concentration is uniform throughout the scaffold depth. Collagen was allowed to polymerize at
145 37 °C and 5% CO_2 for 30 minutes.

146 **Treatment with ephrinA1**

147 Cells seeded in collagen hydrogels were cultured for 24 hours after seeding to allow for cells to
148 engage the collagen and achieve a physiologically relevant morphology. After 24 hours, hydrogels
149 in the ephrin A1 treated condition were cultured in serum-free cell culture media with 1 μ g/ml
150 ephrin A1-FC (R&D Systems) added to the media for 12 hours prior to electroporation treatment
151 or fixation for immunofluorescence staining. Control cells were cultured in hydrogels submerged
152 in serum-free culture media without the added ephrin A1-FC for 12 hours prior to use in
153 experiments. The 12-hour time point was chosen because a full morphological change of the cells
154 within the hydrogels was seen by 12 hours and no further changes were observed at longer
155 exposure times (Fig S2). No difference was seen in viability between hydrogels cultured in ephrin
156 A1-FC conditioned media and control media before exposure to electroporation therapy (Fig S4).

157 **Fluorescent staining**

158 U-87, U251, DBTRG, and NHA cells were individually seeded in hydrogels described previously.
159 After culturing the cells for 24 hours for engagement with the matrix and then an addition 12 hours
160 after treatment, the hydrogels were fixed using 4% formalin and blocked and permeabilized using
161 40 mg/mL bovine serum albumin (BSA) and 0.05% Triton-X. Cellular F-actin was stained with
162 Alexa Flour 568 phalloidin (Life Technologies, Carlsbad, CA) while cell nuclei were stained with
163 diaminophenylindole (DAPI; Sigma-Aldrich, St. Louis, MO). Cells were visualized using a Zeiss
164 LSM880 (Carl Zeiss Microscopy LLC, Thornwood, NY) laser scanning confocal microscope.

165 **Determination of NCR**

166 . Untreated hydrogels seeded at the same cell density and collagen conditions as treated hydrogels
167 were fixed and fluorescently stained to determine overall cell area and nuclear area for cells in the
168 control condition and in the ephA1 treated condition. Measurements were made on at least four
169 cells per hydrogel and at least 5 hydrogels were analyzed for each condition so at least 20 cells
170 were used to determine average NCR for each cell type in each condition. Image analysis was done
171 in Image J (NIH, Bethesda, MD. Z-stack images were converted into 2D projection images and
172 cell measurements were made from these projections. NCR was calculated from the measured cell
173 area (A_C) and nuclear area (A_N) as follows:

174
$$NCR = \frac{A_N}{A_C - A_N} \quad (1)$$

175 **Finite element analysis in hydrogels**

176 Finite element models using COMSOL Multiphysics (Version 4.3, COMSOL Inc., Palo Alto,
177 CA) were used to solve the Laplace equation to find the electric field distribution within the
178 hydrogels for each different voltage used. The electric field distribution within the hydrogel was
179 found by solving the Laplace Equation:

180
$$\nabla^2 \phi = 0 \quad (2)$$

181 where ϕ is the electrical potential. The boundaries of one electrode were set to the applied voltage
182 ($\phi = V_{\text{applied}}$) and the boundaries of the second were set to ground ($\phi = 0$) while the initial voltage
183 (V_0) for all subdomains were set to 0V. All other external boundaries were set to electrical
184 insulation ($-\mathbf{n} \cdot \mathbf{J} = 0$). The mesh was refined until error between successive refinements was less
185 than 1%. The final mesh contained 47,438 elements and solutions were found in approximately
186 3 minutes on a Pentium i3 processor.

187 **Finite element analysis of individual cells based on NCR**

188 The electrodynamic solutions of interest were reached by modeling a spherical cell membrane
189 and nuclear envelope and solving a finite element model with an impedance boundary condition
190 scheme as previously described (25, 30). The models used in to investigate the membrane
191 response to different pulse parameters changed its NCR based on representative cell geometries
192 determined based on average measurements made in ImageJ image analysis software (NIH,
193 Bethesda, MD) from confocal microscopy images. In order to better understand the effect of high
194 frequency components of H-FIRE on individual cells a frequency-dependent module was used to
195 mimic the increase in frequency for different H-FIRE pulse lengths and IRE-type pulses. The
196 geometry and physical properties of the cell can be found in Supplemental Table 2.

197

198 Simulations were solved in the frequency-domain using an electric currents module, which has
199 been previously shown to correlate well for spherical cells exposed to rectangular pulses in the
200 order of 1-2 μ s (28). To account for the impedance posed by the membranes of the cell and
201 nucleus their boundaries were assigned impedance properties found in literature (Supplemental
202 Table 2).

203 **Electroporation techniques**

204 Pulsed electroporation experiments were performed in collagen hydrogels with constant
205 electrical properties. High- frequency pulses were delivered using a custom-built pulse
206 generation system (INSPIRE 2.0, VoltMed Inc., Blacksburg, VA). Pulses were delivered
207 through custom build electrodes composed of two solid stainless steel cylinders with
208 diameters of 0.87 mm, separated 3.3 mm edge-to-edge, with spacing and geometry maintained
209 by a 3D printed electrode holder. In the H-FIRE pulsing protocol, treatments were performed
210 delivering 50 bursts of 1 μ s bipolar pulses. A burst consisted of 100 x 1 μ s pulses of
211 alternating polarity with a 5 μ s inter-pulse delay delivered with a repetition rate of 1 burst per
212 second. Voltage output was set to 700 V to achieve measurable lesions within the hydrogel
213 geometry. Conventional IRE pulses were delivered using an ECM 830 pulse generator
214 (Harvard apparatus, Holliston, MA) through the same custom built electrodes. These
215 treatments consisted of 50 square pulses of 100 μ s pulse width with a repetition rate of 1 pulse
216 per second. IRE voltage output was set to 350 V to achieve measurable lesions within the
217 hydrogel geometry.

218 **Determination of lethal threshold in hydrogels**

219 The thresholds for cell death were determined by first performing a live-dead stain on the
220 hydrogels 24 hours after delivering treatment. Live cells were stained with Calcein AM (Biotium,
221 Hayward, CA) and fluoresced as green while dead cells were stained with ethidium homodimer
222 III (Biotium, Hayward, CA) and fluoresced as red. The size of the red-stained dead region was
223 measured using ImageJ image analysis software. Geometric measurements of the ablation zones
224 were mapped to a finite element model to calculate the electric field during treatments of the
225 scaffolds. The electric field magnitude at the edge of the live and dead regions was considered the
226 electric field threshold for cell death for the given cell type. **Each individual hydrogel exposed to**

227 either H-FIRE therapy or H-FIRE with eA1 therapy measured to determine the lethal electric field
228 for the cell type was considered an independent sample representing the response of approximately
229 125000 cells. For each condition, hydrogels were pulsed in at least 3 different independent
230 experiments on different days.

231 **Power spectral analysis**

232 A power spectral analysis was conducted by running a Fast Fourier Transform (FFT) on the
233 experimental H-FIRE pulses. The power spectral analysis was used to determine the dominant
234 frequencies a cell is exposed to upon treatment as demonstrated elsewhere as a tool for
235 understanding bipolar pulses (31).

236 **Statistical analysis**

237 Statistical significance was determined by a two-tailed *t*-test performed in Prism Statistical
238 Software (Version 6, Graphpad, La Jolla, CA). A 95% confidence interval was used with
239 significance defined as $p < 0.05$. All numerical results are reported as the mean and the standard
240 deviation of all experimental measurements. No outliers were excluded.

241 **Data Availability**

242 The datasets generated during and analyzed during the current study are available from the
243 corresponding author on reasonable request.

244

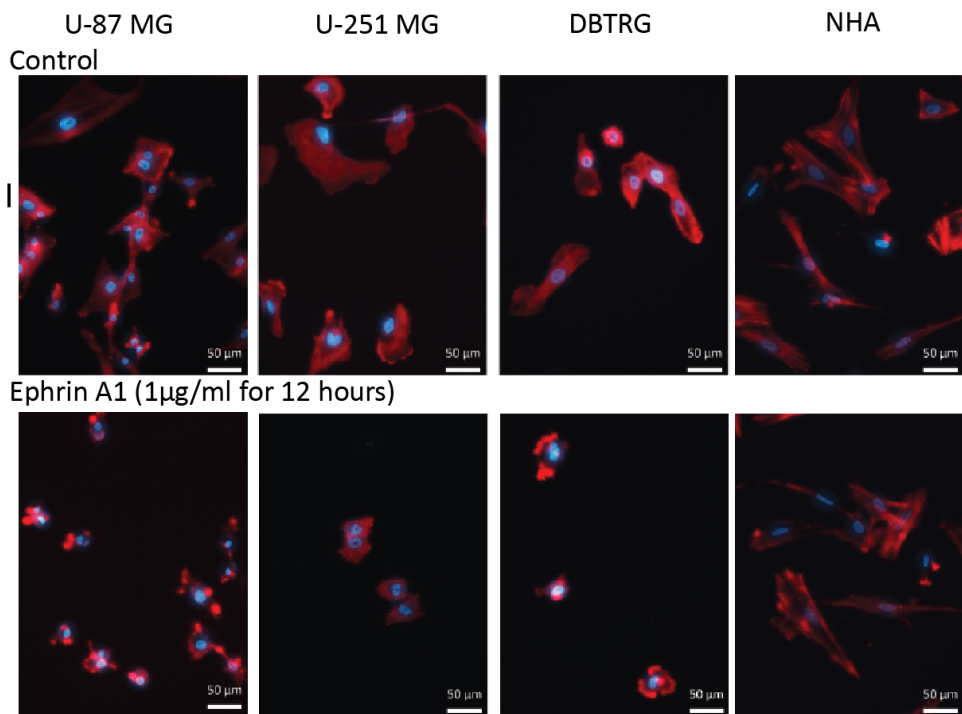
245 **Results**

246 **EphA2 activation by eA1 induces a targeted morphology change in malignant cells**

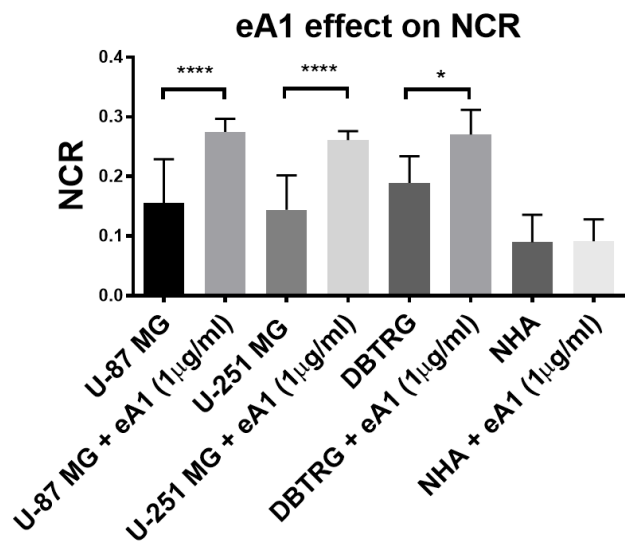
247 To investigate the dynamics of eA1 induced morphology changes, we cultured malignant GBM
248 and normal brain cells in 3D hydrogels and exposed them to eA1. EphA2 activation by eA1 in
249 malignant cell lines (U-87 MG, U-251 MG, and DBTRG) led to visible cell morphology changes

250 characterized by cell rounding and a collapse of the cytoplasm (Fig 1a). Cell rounding was visible
251 after 6 hours of culture in media containing eA1 (1 μ g/ml) with the full morphological change
252 accomplished by 12 hours (Fig S2). In normal human astrocyte (NHA) cells, no morphological
253 change was observed at any time point out to 48 hours when culturing hydrogels in eA1 media.
254 For the malignant cell lines, the cytoplasm collapse upon EphA2 activation resulted in a significant
255 change in the NCR of the cells (Fig 1b). NHA cells showed no significant change in NCR under
256 these treatment conditions. No morphology change was observed in control tumor cells cultured
257 in media without eA1 present.

a



b



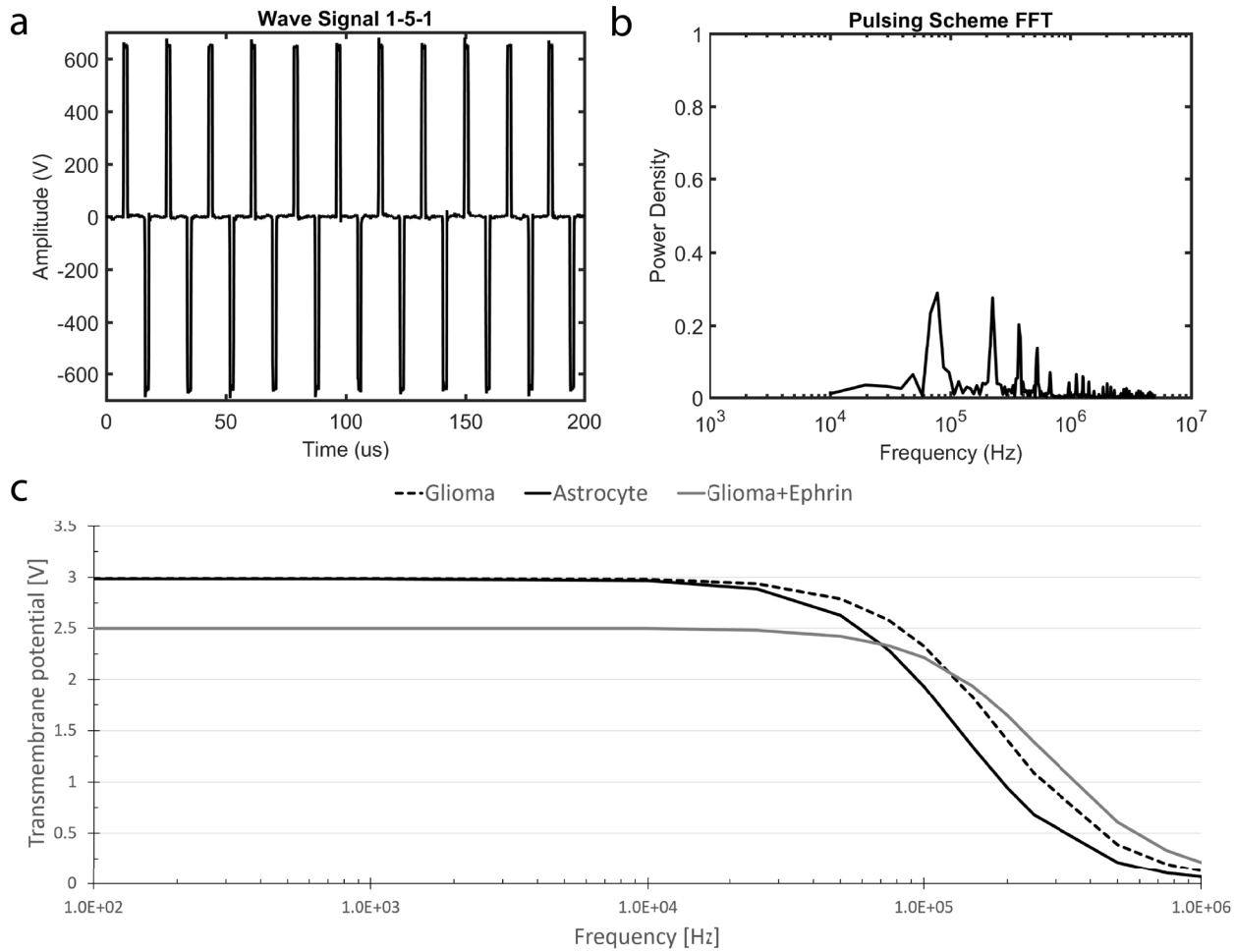
258

259 **Figure 1. Treatment with soluble ephrin A1 causes glioma morphology change, while not altering NCR for**
260 **astrocytes. (a)** Malignant cells stain with DAPI (blue) and phalloidin (red) cultured in media with 1 μ g/ml eA1 for 12
261 hours exhibit cell rounding and a collapse of the cytoplasm around the nucleus while healthy cell morphology remains
262 unchanged upon exposure to eA1. Scale bar 50 μ m (b) eA1 induced morphology change results in a quantitative
263 increase in NCR for malignant cells while NCR remains unchanged for normal astrocytes. (n=20) ****p \leq 0.0001,
264 *p=0.027

265

266

267
268 **Extent of electroporation for different cell morphologies is dependent on frequency of**
269 **electric field**
270 Finite element modeling was used to predict the induced TMP on a variety of cell morphologies
271 as a function of the frequency of a steady-state, AC electric field. Characteristic morphologies
272 determined from experimental culture of glioma cells, normal astrocytes, and glioma cells treated
273 with eA1 were used. At lower frequencies, characteristic of IRE pulse waveforms, larger cells
274 experience a greater induced transmembrane potential compared with a glioma cell that shrinks
275 in volume due to treatment with eA1. At a frequency of approximately 10 kHz, the enlarged
276 nucleus of the glioma cell causes it to experience a greater transmembrane potential than the
277 astrocyte of the same size but smaller nucleus. This trend continued throughout higher
278 frequencies of electric field, suggesting that fields of frequency higher than 10 kHz can be used
279 to accomplish greater electroporation on cells with a larger nucleus than in cells with a smaller
280 nucleus. At an electric field frequency of approximately 100 kHz the smaller cell experiences a
281 larger induced transmembrane potential than the larger cells, suggesting a greater extent of
282 electroporation of smaller cells than larger cells.



283
284
285 **Figure 2. a) Experimental pulse waveform applied to hydrogels.** A bipolar waveform of 1 μ s pulses separated by a
286 5 μ s delay was used to accomplish electroporation in hydrogel platform b) **Power spectrum analysis of experimental**
287 **pulse train.** Amplitude frequency distribution found by Fast Fourier Transform of experimental pulse trains shows
288 that the pulse train of 1 μ s bipolar pulses separated by a 5 μ s delay delivers the majority of its power in the frequencies
289 around 100 kHz. c) **Single cell steady-state response to electric field of 1000V/cm applied as AC signal.** As expected,
290 larger cells (U87 and Astrocyte) present larger TMP's at lower frequencies. However, cells of higher NCR will have
291 larger TMP's at higher frequencies (>100kHz).
292

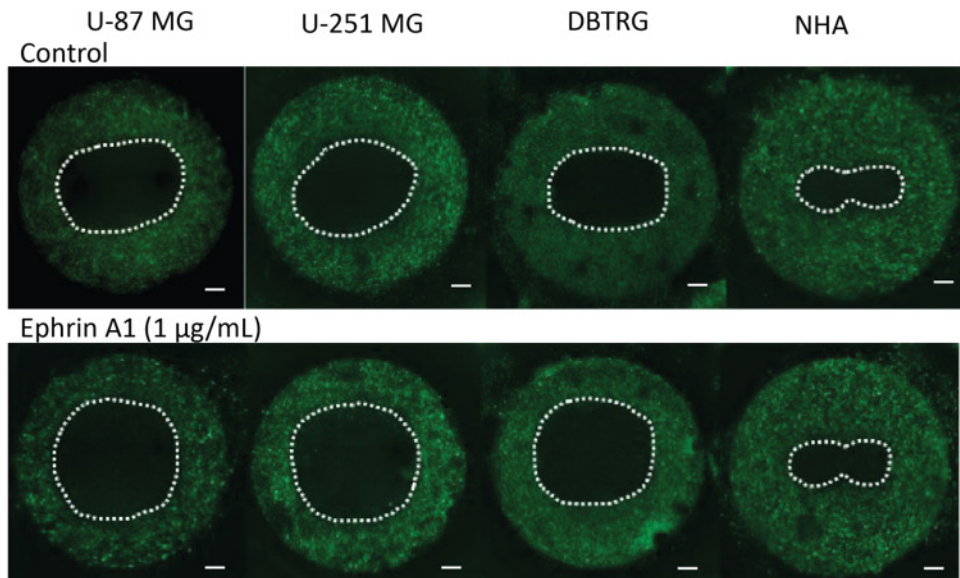
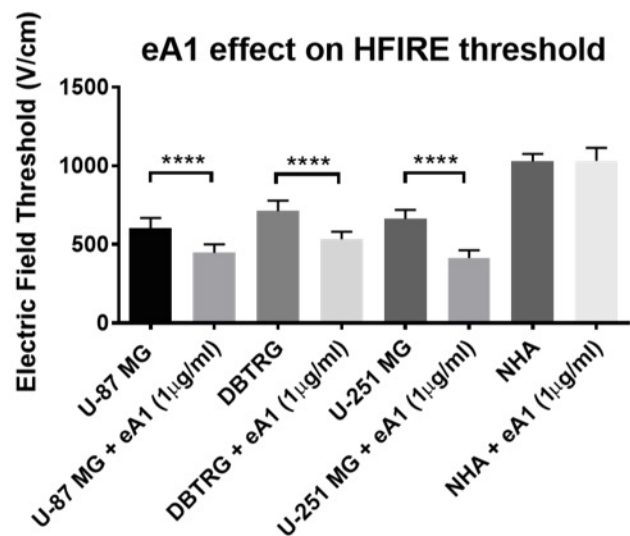
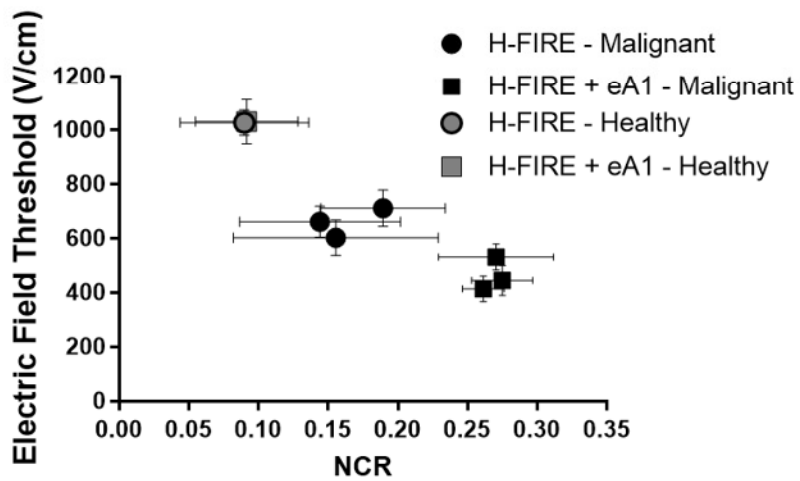
293 As the duration of the applied pulse is decreased, a greater proportion of the power is concentrated
294 in higher frequency signal content. The experimental pulse train of 1 μ s bipolar pulses with a 5 μ s
295 delay between pulses (Fig 2a), delivers the majority of its power between 100 kHz and 1000 kHz
296 (Fig 2b). Interestingly, these frequencies correspond to the frequencies predicted to allow for a
297 cross-over in TMP for the eA1-induced cell morphologies when exposed to an AC signal (Fig 2c).
298

299 **Morphology change impacts lethal thresholds for electroporation of malignant cells**

300 To determine if the increase in NCR in malignant cells led to a change in H-FIRE threshold as
301 predicted by finite element modeling, eA1 treated hydrogels were exposed to a regimen of H-FIRE
302 treatment and compared with control hydrogels. Malignant hydrogels treated with eA1 had
303 significantly larger lesions than control hydrogels while non-malignant hydrogels had no
304 significant difference between conditions (Fig 3a). The increase in NCR for malignant cells
305 corresponded to a smaller lethal threshold for H-FIRE while the lethal threshold did not change
306 for non-malignant cells (Fig 3b). For U87 cells, under normal conditions the lethal threshold is
307 603 ± 65 V/cm (n=8) while treated with eA1 the lethal threshold is 446 ± 55 V/cm (n=8). For U-
308 251 cells, under normal conditions the lethal threshold is 662 ± 57 V/cm (n=8) while treated with
309 eA1 the lethal threshold is 415 ± 48 V/cm (n=8). For DBTRG cells, under normal conditions the
310 lethal threshold is 712 ± 68 V/cm (n=6) while treated with eA1 the lethal threshold is 532 ± 48
311 V/cm (n=6). Lethal thresholds for non-malignant cell types remained unchanged. Control NHA
312 cells are killed at a threshold of 1028 ± 47 V/cm (n=6) and eA1 treated NHA cells have a lethal
313 threshold of 1032 ± 82 V/cm (n=6). For the most responsive cell type, U-251 cells, eA1 treatment
314 resulted in a 37% decrease in lethal threshold for H-FIRE therapy.

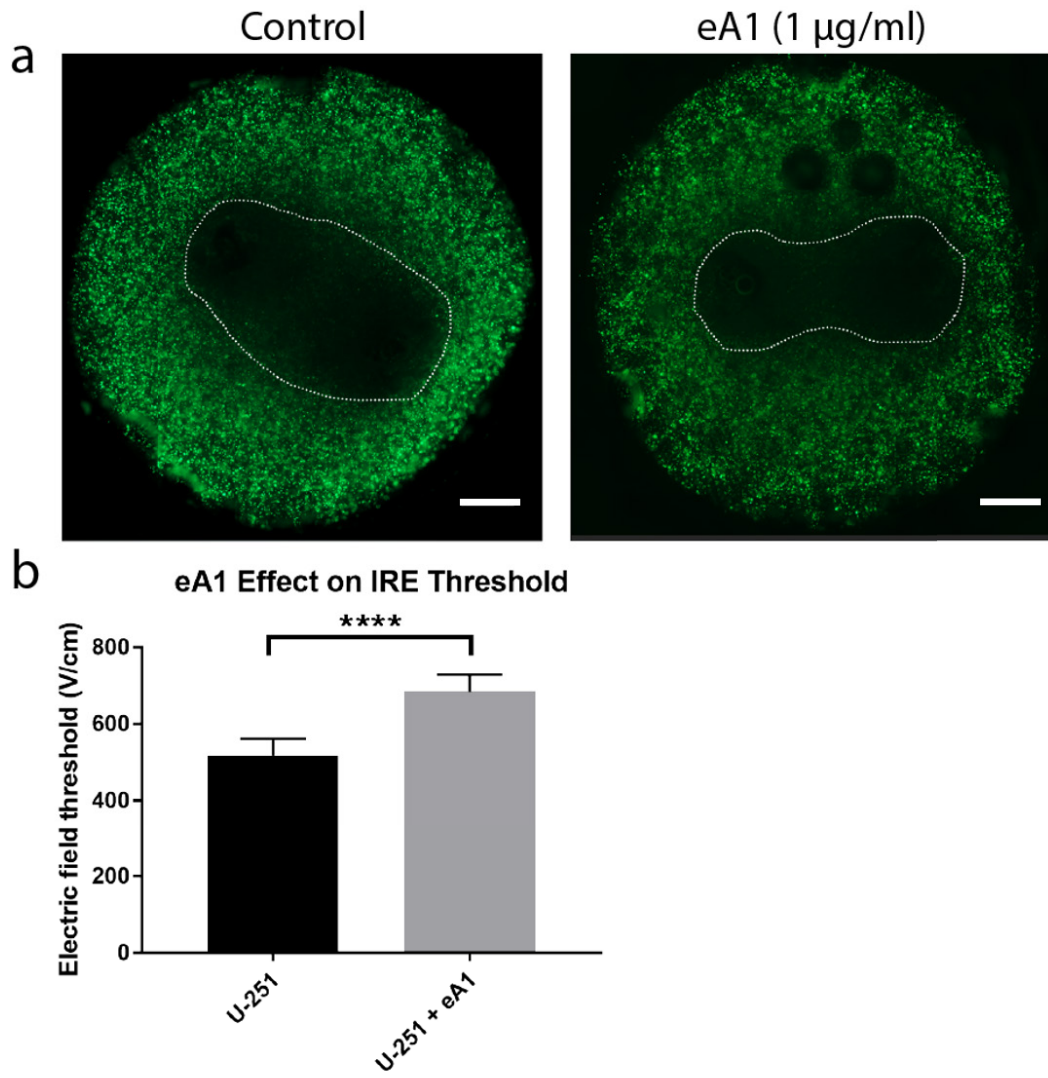
315

316

a**b****c**

318 **Figure 3. NCR change induced by ephrinA1 enhances H-FIRE lesions in malignant cells. (a)** H-FIRE lesion size
319 for malignant glioma cells (U-87, U-251, and DBTRG) is increased from control when hydrogels are cultured with
320 eA1 ligand. H-FIRE lesions in non-malignant astrocytes (NHA) remain unchanged with eA1 exposure. Scale bar 1
321 mm **(b)** COMSOL modeling relating lesion size to lethal thresholds shows a significant decrease in H-FIRE lethal
322 threshold for malignant cells when treated with eA1 prior to electroporation exposure. H-FIRE lethal threshold for
323 non-malignant cells remains unchanged with eA1 exposure. **(c)** Summary of data shows a correlation between average
324 NCR of a given cell type in the hydrogel and the lethal electric field threshold for that cell type in the hydrogel. Healthy
325 astrocytes (gray markers) show no change with eA1 treatment while malignant cells (black markers) show a
326 decreased lethal electric field threshold when treated with eA1 to induce an NCR increase. ***p ≤ 0.0001
327

328 Similarly, eA1 treated hydrogels were exposed to traditional IRE pulses of 100 μ s pulse width to
329 determine if these lesions would change as a result of the eA1-induced morphology change in
330 treated cells. In contrast to the trend seen using H-FIRE pulses, IRE lesions of eA1-treated U-251
331 cells are significantly smaller than control hydrogels of U-251 cells cultured in normal media (Fig
332 4). U-251 cells cultured in normal media within the hydrogels had an IRE lethal threshold of 517
333 \pm 45 V/cm (n=6). U-251 cells cultured with media containing 1 μ g/ml eA1 within the hydrogels
334 had an IRE lethal threshold of 684 \pm 44 V/cm (n=6).



335

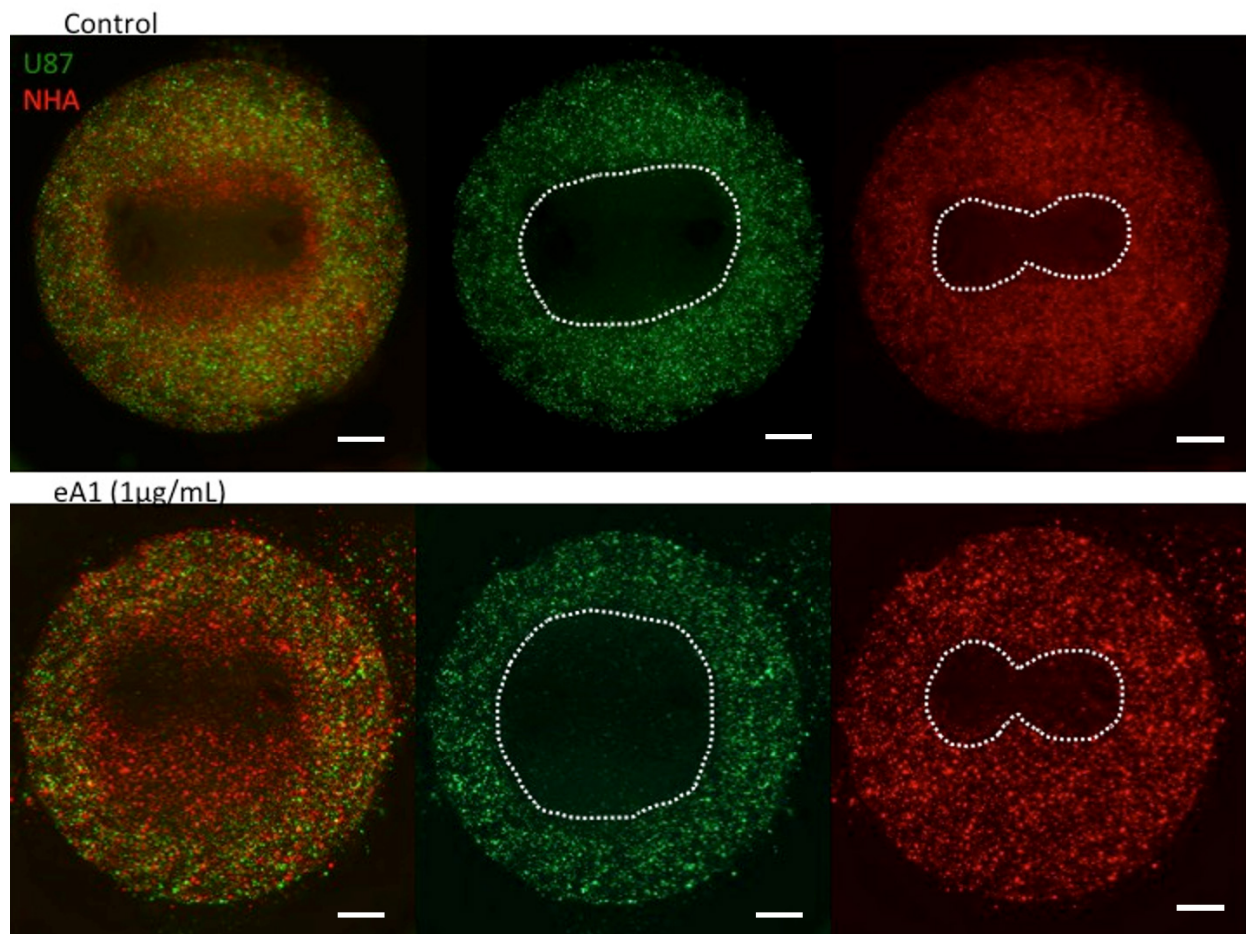
336 **Figure 4. NCR change induced by ephrinA1 results in smaller IRE lesions.** (a) IRE lesion size for U-251 glioma
 337 cells is smaller compared to the control when hydrogels are cultured with eA1 ligand. Scale bars 1 mm. (b) COMSOL
 338 modeling relating lesion size to lethal thresholds shows a significant increase in IRE lethal threshold for U-251 cells
 339 when treated with eA1 prior to electroporation exposure.(n=6) ****p \leq 0.0001
 340

341 **eA1 treatment enhances malignant cell selectivity of H-FIRE**

342 To demonstrate the enhanced selectivity of malignant cells possible with combination H-FIRE and
 343 eA1 treatment, we performed co-culture experiments. Hydrogels of NHAs and U-87 GBM cells
 344 were cultured in media containing eA1 and then exposed to a regime of H-FIRE pulses. While
 345 selective killing of U87 cells and not NHA cells is achieved in the control condition, the region of

346 U87 killing is significantly enlarged while the NHA lesion remains the same for cells exposed to
347 eA1 (Fig 5).

348



349

350 **Figure 5. Treatment with eA1 enhances selectivity of H-FIRE for malignant cells in co-culture.** The area of ablated
351 malignant cells and live healthy cells in extended by treating co-culture hydrogels with eA1 prior to H-FIRE exposure.
352 Scale bars 1 mm.

353

354

355 Discussion

356 We have demonstrated that the cell size dependence for electroporation-induced cell death depends
357 critically on frequency range. Each component of the cell—membrane, cytoplasm, and nuclear
358 membrane—has a characteristic impedance that affects the TMP response to varying degrees
359 depending on the cell morphology. As the capacitance of each part of the cell is dependent on the

360 surface area, the change in morphology induced by eA1 treatment will produce changes in cell
361 capacitance.

362

363 We hypothesize that the effect demonstrated here of high frequency PEFs preferentially ablating
364 cells of smaller volume but higher NCR may be due to changes in impedance of the cytoplasm. If
365 part of the external field is able to bypass the cell membrane and interact with internal components
366 of the cell, the impedance of the cytoplasm and nucleus become important factors. This effect will
367 be magnified as the volume of the cytoplasm is decreased, which can be exploited through
368 treatment with eA1. Therefore, for high frequency pulses, the NCR of a cell becomes a significant
369 variable in predicting electroporation response. This finding is significant for the understanding of
370 electroporation theory because it clearly illustrates that the relationship between cell size and
371 electroporation is closely dependent on waveform frequency, which would impact electroporation
372 protocols both for research as well as therapeutic applications.

373

374 We have shown for the first time that molecular targeting with ensuing changes in GBM cell
375 morphology may be used to enhance the selectivity of PEFs to induce tumor cell death. Selectivity,
376 regulated by NCR, opens up the possibility of enhanced targeted cancer therapy, as malignant cells
377 are known to often have increased NCR compared to normal cells (32, 33). Because the EphA2
378 receptor is overexpressed specifically on malignant cells in adulthood, the induced morphology
379 change can be exploited in developing combinatorial targeted therapies using H-FIRE. The ability
380 to selectively target cells with increased NCR is significant for the future of GBM treatment
381 because it may allow for the treatment of diffuse malignant cells that have invaded into normal
382 brain tissue. By lowering the lethal threshold for malignant cells in the outermost regions of the

383 tumor where selectivity is most important, eA1 treatment may increase the margin of tumor that
384 can safely be ablated with H-FIRE therapy regimes. Though many attempts have been made to use
385 EphA2 as a direct therapeutic target (19, 34), this work is the first to our knowledge that utilizes a
386 resulting morphological change to enhance targeting by combination with a physical therapy in
387 the form of PEFs. We furthermore note that short pulses ($\sim 1 \mu\text{s}$) pulses in particular are necessary
388 to induce this synergistic tumor cell death response, as we have demonstrated that longer (~ 100
389 μs) IRE pulses of the sort most commonly used for clinical tumor ablation (5, 7) become less
390 effective in combination with sub-lethal eA1 treatment in our studies. Though this work represents
391 the early stages of cell-selective electroporation techniques, the results presented here suggests the
392 ability to optimize parameters to further increase the selectivity with the possibility of efficacy in
393 an in vivo context. The performed power spectral analysis of IRE and H-FIRE pulses indicates
394 that a higher frequency signal content ($> 100 \text{ kHz}$) may increase our ability to target cells of a
395 higher NCR. While this analysis offers some insight to the mechanism for cell targeting of HFIRE,
396 future work in the development of an accurate time-domain model is warranted.

397

398

399

400

401 The EphA2 receptor has been identified as overexpressed in various cancers (35-39) in addition
402 to GBM, suggesting the broader application of our results for treatments in other tumor sites for
403 which more traditional surgical or radiotherapy options may be limited, for example tumors that
404 surround sensitive nerve or vascular structures. Areas of increased EphA2 expression are
405 important therapy targets as elevated EphA2 expression has been correlated with higher

406 pathological grade (40) and poor prognosis (41, 42). EphA2 is an important target for this
407 synergistic therapy for another important reason, specifically that it may allow for the targeting
408 of highly tumorigenic glioma stem cells (GSCs), which ECT combinatorial treatments may leave
409 behind due to their highly chemo-resistant nature (43). EphA2 receptors have been found to be
410 expressed most highly on tumor initiating cells with the highest levels of expression in the most
411 aggressive, stem cell-like mesenchymal subtype (44). Though the EphA2/ephrinA1 interaction
412 has been the subject of our study, multi-ligand cocktails can also be explored to capitalize on the
413 other ephrin interactions in cancer.

414

415 The findings presented here highlight the importance of considering the physical phenotypes of
416 cells both for treatment planning and for exploitation to improve treatment efficacy. The classical
417 understanding of electroporation simplifies the relationship between TMP and cell shape and size.
418 However, we have shown that the relationship is more complex, and the vast pulse frequency
419 parameter space should be further explored to identify novel therapeutic synergies of the sort that
420 we have demonstrated here. Taking into account the complex relationship between these variables
421 may open up the possibility for significantly improved cancer therapies by targeting the physical
422 hallmarks of tumor cells with next generation combinatorial therapies. Though our findings are
423 presented here in the context of tumor ablation, the importance of considering cellular biophysics
424 extends to other applications of electroporation as well. Applications such as genetic engineering
425 may benefit from manipulating cellular biophysics to more effectively deliver intracellular cargo
426 both in therapy applications but also as a practice in basic research.

427

428 **Acknowledgements**

429 We would like to express our gratitude to Daniel Sweeney for useful discussions and assistance
430 understanding analytical models of electroporation. This work was supported by the National
431 Cancer Institute of the National Institutes of Health through awards R21CA192042 and
432 R01CA213423, by National Science Foundation CAREER (CBET-1652112) and REU (EEC-
433 1359073) awards, and by Wake Forest Comprehensive Cancer Center proposal development
434 pilot funds.

435

436 **Author Contributions**

437 J.W.I.: study design, cell culture, 3D scaffolds construction, confocal microscopy imaging, live
438 dead staining, mathematical modeling, data analysis and interpretation, writing of manuscript.
439 E.L.L: construction of custom electronics, finite element modeling, data analysis and
440 interpretation, writing of manuscript. M.L.R.: cell culture, 3D scaffolds construction, live dead
441 staining, data analysis G.J.L.: conception of project plan W.D.: conception of project plan, study
442 design R.V.D.: conception of project plan, study design, data analysis and interpretation, writing
443 of manuscript. S.S.V.: conception of project plan, study design, data analysis and interpretation,
444 writing of manuscript.

445 **References**

- 446 1. Weaver, J. C., and Y. A. Chizmadzhev. 1996. Theory of electroporation: A review.
447 *Bioelectrochemistry and Bioenergetics* 41:135-160.
- 448 2. Mir, L. M. 2001. Therapeutic perspectives of in vivo cell electroporabilization.
449 *Bioelectrochemistry* 53:1-10.
- 450 3. Agerholm-Larsen, B., H. K. Iversen, P. Ibsen, J. M. Moller, F. Mahmood, K. S. Jensen, and J. Gehl.
451 2011. Preclinical validation of electrochemotherapy as an effective treatment for brain tumors.
452 *Cancer research* 71:3753-3762.
- 453 4. Davalos, R. V., L. Mir, and B. Rubinsky. 2005. Tissue ablation with irreversible electroporation.
454 *Annals of biomedical engineering* 33:223-231.
- 455 5. Cannon, R., S. Ellis, D. Hayes, G. Narayanan, and R. C. Martin. 2013. Safety and early efficacy of
456 irreversible electroporation for hepatic tumors in proximity to vital structures. *Journal of surgical*
457 *oncology* 107:544-549.

458 6. Onik, G., and B. Rubinsky. 2010. Irreversible electroporation: first patient experience focal
459 therapy of prostate cancer. In *Irreversible Electroporation*. Springer. 235-247.

460 7. Martin, R. C., D. Kwon, S. Chalikonda, M. Sellers, E. Kotz, C. Scoggins, K. M. McMasters, and K.
461 Watkins. 2015. Treatment of 200 locally advanced (stage III) pancreatic adenocarcinoma
462 patients with irreversible electroporation: safety and efficacy. *Annals of surgery* 262:486-494.

463 8. Neal, R. E., J. L. Millar, H. Kavnoudias, P. Royce, F. Rosenfeldt, A. Pham, R. Smith, R. V. Davalos,
464 and K. R. Thomson. 2014. In vivo characterization and numerical simulation of prostate
465 properties for non-thermal irreversible electroporation ablation. *The Prostate* 74:458-468.

466 9. Lee, E. W., C. Chen, V. E. Prieto, S. M. Dry, C. T. Loh, and S. T. Kee. 2010. Advanced hepatic
467 ablation technique for creating complete cell death: irreversible electroporation 1. *Radiology*
468 255:426-433.

469 10. Guo, Y., Y. Zhang, R. Klein, G. M. Nijm, A. V. Sahakian, R. A. Omary, G.-Y. Yang, and A. C. Larson.
470 2010. Irreversible electroporation therapy in the liver: longitudinal efficacy studies in a rat
471 model of hepatocellular carcinoma. *Cancer research* 70:1555-1563.

472 11. Daniels, C., and B. Rubinsky. 2009. Electrical field and temperature model of nonthermal
473 irreversible electroporation in heterogeneous tissues. *Journal of biomechanical engineering*
474 131:071006.

475 12. Lee, E. W., C. T. Loh, and S. T. Kee. 2007. Imaging guided percutaneous irreversible
476 electroporation: ultrasound and immunohistological correlation. *Technology in cancer research
& treatment* 6:287-293.

477 13. Bonakdar, M., E. L. Latouche, R. L. Mahajan, and R. V. Davalos. 2015. The feasibility of a smart
478 surgical probe for verification of ire treatments using electrical impedance spectroscopy. *ieee T
479 Bio-Med Eng* 62:2674-2684.

480 14. Neal II, R., J. Rossmeisl Jr, V. D'Alfonso, J. Robertson, P. Garcia, S. Elankumaran, and R. Davalos.
481 2014. In vitro and numerical support for combinatorial irreversible electroporation and
482 electrochemotherapy glioma treatment. *Annals of biomedical engineering* 42:475-487.

483 15. Wykosky, J., D. M. Gibo, C. Stanton, and W. Debinski. 2005. EphA2 as a Novel Molecular Marker
484 and Target in Glioblastoma Multiforme. *Molecular Cancer Research* 3:541-551.

485 16. Hatano, M., J. Eguchi, T. Tatsumi, N. Kuwashima, J. E. Dusak, M. S. Kinch, I. F. Pollack, R. L.
486 Hamilton, W. J. Storkus, and H. Okada. 2005. EphA2 as a Glioma-Associated Antigen: A Novel
487 Target for Glioma Vaccines. *Neoplasia* 7:717-722.

488 17. Liu, D.-P., Y. Wang, H. P. Koeffler, and D. Xie. 2007. Ephrin-A1 is a negative regulator in glioma
489 through down-regulation of EphA2 and FAK. *International journal of oncology* 30:865-872.

490 18. Wykosky, J., E. Palma, D. Gibo, S. Ringler, C. Turner, and W. Debinski. 2008. Soluble monomeric
491 EphrinA1 is released from tumor cells and is a functional ligand for the EphA2 receptor.
492 *Oncogene* 27:7260-7273.

493 19. Wykosky, J., D. M. Gibo, and W. Debinski. 2007. A novel, potent, and specific ephrinA1-based
494 cytotoxin against EphA2 receptor-expressing tumor cells. *Molecular cancer therapeutics* 6:3208-
495 3218.

496 20. Ferluga, S., R. Hantgan, Y. Goldgur, J. P. Himanen, D. B. Nikolov, and W. Debinski. 2013.
497 Biological and Structural Characterization of Glycosylation on Ephrin-A1, a Preferred Ligand for
498 EphA2 Receptor Tyrosine Kinase. *The Journal of Biological Chemistry* 288:18448-18457.

499 21. Miao, H., E. Burnett, M. Kinch, E. Simon, and B. Wang. 2000. Activation of EphA2 kinase
500 suppresses integrin function and causes focal-adhesion-kinase dephosphorylation. *Nature cell
501 biology* 2:62-69.

502 22. Eppich, H. M., R. Foxall, K. Gaynor, D. Dombkowski, N. Miura, T. Cheng, S. Silva-Arrieta, R. H.
503 Evans, J. A. Mangano, F. I. Preffer, and D. T. Scadden. 2000. Pulsed electric fields for selection of
504 hematopoietic cells and depletion of tumor cell contaminants. *Nat Biotech* 18:882-887.

505

506 23. Agarwal, A., I. Zudans, E. A. Weber, J. Olofsson, O. Orwar, and S. G. Weber. 2007. Effect of cell
507 size and shape on single-cell electroporation. *Analytical chemistry* 79:3589-3596.

508 24. Van den Bos, W., D. de Bruin, B. Muller, I. Varkarakis, A. Karagiannis, P. Zondervan, M. L. Pes, D.
509 Veelo, C. S. Heijink, and M. Engelbrecht. 2014. The safety and efficacy of irreversible
510 electroporation for the ablation of prostate cancer: a multicentre prospective human *in vivo*
511 pilot study protocol. *BMJ open* 4:e006382.

512 25. Ivey, J. W., E. L. Latouche, M. B. Sano, J. H. Rossmeisl, R. V. Davalos, and S. S. Verbridge. 2015.
513 Targeted cellular ablation based on the morphology of malignant cells. *Scientific reports* 5.

514 26. Arena, C. B., M. B. Sano, J. H. Rossmeisl, J. L. Caldwell, P. A. Garcia, M. N. Rylander, and R. V.
515 Davalos. 2011. High-frequency irreversible electroporation (H-FIRE) for non-thermal ablation
516 without muscle contraction. *Biomedical engineering online* 10:102.

517 27. Cross, V. L., Y. Zheng, N. W. Choi, S. S. Verbridge, B. A. Sutermaster, L. J. Bonassar, C. Fischbach,
518 and A. D. Stroock. 2010. Dense type I collagen matrices that support cellular remodeling and
519 microfabrication for studies of tumor angiogenesis and vasculogenesis *in vitro*. *Biomaterials*
520 31:8596-8607.

521 28. Sano, M. B., C. B. Arena, M. R. DeWitt, D. Saur, and R. V. Davalos. 2014. In-vitro bipolar nano-
522 and microsecond electro-pulse bursts for irreversible electroporation therapies.
523 *Bioelectrochemistry* 100:69-79.

524 29. White, F., and K. Gohari. 1981. Variations in the nuclear-cytoplasmic ratio during epithelial
525 differentiation in experimental oral carcinogenesis. *Journal of Oral Pathology & Medicine*
526 10:164-172.

527 30. Jin, Y., L. Yang, and F. White. 1995. Preliminary assessment of the epithelial nuclear-cytoplasmic
528 ratio and nuclear volume density in human palatal lesions. *Journal of oral pathology & medicine*
529 24:261-265.

530 31. Parri, M., M. L. Taddei, F. Bianchini, L. Calorini, and P. Chiarugi. 2009. EphA2 Reexpression
531 Prompts Invasion of Melanoma Cells Shifting from Mesenchymal to Amoeboid-like Motility
532 Style. *Cancer Research* 69:2072-2081.

533 32. Faoro, L., P. A. Singleton, G. M. Cervantes, F. E. Lennon, N. W. Choong, R. Kanteti, B. D.
534 Ferguson, A. N. Husain, M. S. Tretiakova, N. Ramnath, E. E. Vokes, and R. Salgia. 2010. EphA2
535 Mutation in Lung Squamous Cell Carcinoma Promotes Increased Cell Survival, Cell Invasion,
536 Focal Adhesions, and Mammalian Target of Rapamycin Activation. *The Journal of Biological
537 Chemistry* 285:18575-18585.

538 33. Guo, H., H. Miao, L. Gerber, J. Singh, M. F. Denning, A. C. Gilliam, and B. Wang. 2006. Disruption
539 of EphA2 Receptor Tyrosine Kinase Leads to Increased Susceptibility to Carcinogenesis in Mouse
540 Skin. *Cancer Research* 66:7050-7058.

541 34. Taddei, M. L., M. Parri, A. Angelucci, B. Onnis, F. Bianchini, E. Giannoni, G. Raugei, L. Calorini, N.
542 Rucci, and A. Teti. 2009. Kinase-dependent and-independent roles of EphA2 in the regulation of
543 prostate cancer invasion and metastasis. *The American journal of pathology* 174:1492-1503.

544 35. Boyd, A. W., P. F. Bartlett, and M. Lackmann. 2014. Therapeutic targeting of EPH receptors and
545 their ligands. *Nature reviews Drug discovery* 13:39-62.

546 36. Pasquale, E. B. 2010. Eph receptors and ephrins in cancer: bidirectional signalling and beyond.
547 *Nat Rev Cancer* 10:165-180.

548 37. Miao, H., and B. Wang. 2012. EphA receptor signaling—Complexity and emerging themes.
549 *Seminars in Cell & Developmental Biology* 23:16-25.

550 38. Zelinski, D. P., N. D. Zantek, J. C. Stewart, A. R. Irizarry, and M. S. Kinch. 2001. EphA2
551 overexpression causes tumorigenesis of mammary epithelial cells. *Cancer research* 61:2301-
552 2306.

553 39. Miyazaki, T., H. Kato, M. Fukuchi, M. Nakajima, and H. Kuwano. 2003. EphA2 overexpression
554 correlates with poor prognosis in esophageal squamous cell carcinoma. International journal of
555 cancer 103:657-663.

556 40. Thaker, P. H., M. Deavers, J. Celestino, A. Thornton, M. S. Fletcher, C. N. Landen, M. S. Kinch, P.
557 A. Kiener, and A. K. Sood. 2004. EphA2 expression is associated with aggressive features in
558 ovarian carcinoma. Clinical Cancer Research 10:5145-5150.

559 41. Li, X., Y. Wang, Y. Wang, Z. Haining, H. Yang, F. Zhou, J. Zhang, W. Liu, Y. Wang, and X. Zhang.
560 2007. Expression of EphA2 in Human Astrocytic Tumors: Correlation with Pathologic Grade,
561 Proliferation and Apoptosis. Tumor Biology 28:165-172.

562 42. Wang, L.-F., E. Fokas, M. Bieker, F. Rose, P. Rexin, Y. Zhu, A. Pagenstecher, R. Engenhart-Cabillic,
563 and H.-X. An. 2008. Increased expression of EphA2 correlates with adverse outcome in primary
564 and recurrent glioblastoma multiforme patients. Oncology reports 19:151-156.

565 43. Liu, F., P. J. Park, W. Lai, E. Maher, A. Chakravarti, L. Durso, X. Jiang, Y. Yu, A. Brosius, and M.
566 Thomas. 2006. A genome-wide screen reveals functional gene clusters in the cancer genome
567 and identifies EphA2 as a mitogen in glioblastoma. Cancer research 66:10815-10823.

568 44. Liu, G., X. Yuan, Z. Zeng, P. Tunici, H. Ng, I. R. Abdulkadir, L. Lu, D. Irvin, K. L. Black, and S. Y. John.
569 2006. Analysis of gene expression and chemoresistance of CD133+ cancer stem cells in
570 glioblastoma. Molecular cancer 5:67.

571 45. Binda, E., A. Vissioli, F. Giani, G. Lamorte, M. Copetti, K. L. Pitter, J. T. Huse, L. Cajola, N. Zanetti,
572 and F. DiMeco. 2012. The EphA2 receptor drives self-renewal and tumorigenicity in stem-like
573 tumor-propagating cells from human glioblastomas. Cancer cell 22:765-780.

574 46. Grosse, C., and H. P. Schwan. 1992. Cellular membrane potentials induced by alternating fields.
575 Biophysical journal 63:1632.

576 47. Tsong, T. Y. 1990. Electrical modulation of membrane proteins: enforced conformational
577 oscillations and biological energy and signal transductions. Annual review of biophysics and
578 biophysical chemistry 19:83-106.

579 48. Rubinsky, B. 2007. Irreversible electroporation in medicine. Technology in cancer research &
580 treatment 6:255-259.

581 49. Asami, K., Y. Takahashi, and S. Takashima. 1989. Dielectric-Properties of Mouse Lymphocytes
582 and Erythrocytes. Biochim Biophys Acta 1010:49-55.

583 50. Yang, J., Y. Huang, X. J. Wang, X. B. Wang, F. F. Becker, and P. R. C. Gascogne. 1999. Dielectric
584 properties of human leukocyte subpopulations determined by electrorotation as a cell
585 separation criterion. Biophysical Journal 76:3307-3314.

586 51. Gascogne, P. R. C., R. Pethig, J. P. H. Burt, and F. F. Becker. 1993. Membrane-Changes
587 Accompanying the Induced-Differentiation of Friend Murine Erythroleukemia-Cells Studied by
588 Dielectrophoresis. Biochim Biophys Acta 1149:119-126.

589 52. Sano, M. B., E. A. Henslee, E. M. Schmelz, and R. V. Davalos. 2011. Contactless dielectrophoretic
590 spectroscopy: Examination of the dielectric properties of cells found in blood. Electrophoresis
591 32:3164-3171.

592 53. Alberts, B., D. Bray, J. Lewis, M. Raff, K. Roberts, J. D. Watson, and A. Grimstone. 1995.
593 Molecular Biology of the Cell (3rd edn). Trends in Biochemical Sciences 20:210-210.

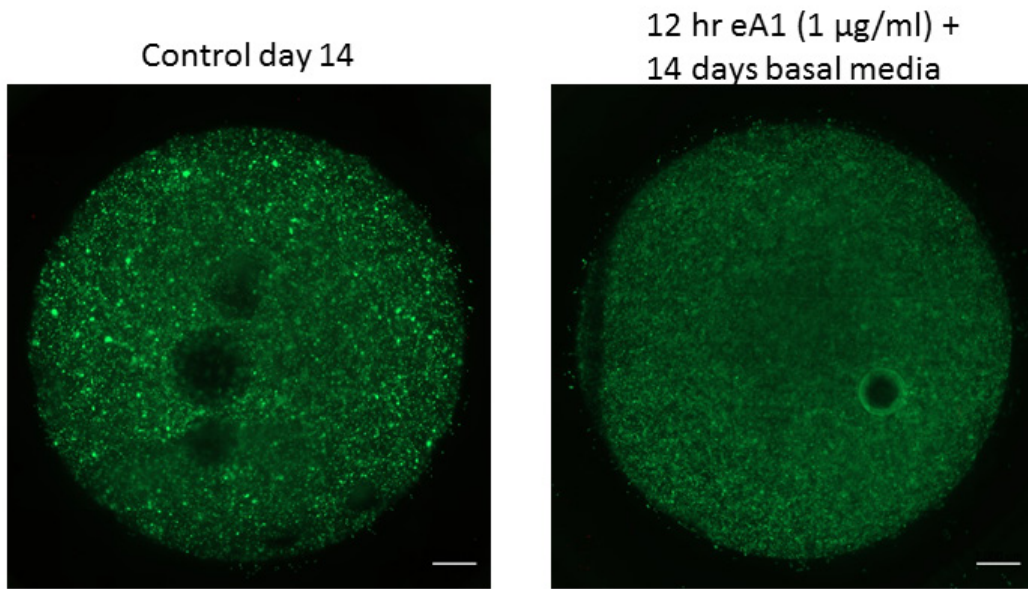
594 54. Huang, S.-H., L.-Y. Hung, and G.-B. Lee. 2016. Continuous nucleus extraction by optically-induced
595 cell lysis on a batch-type microfluidic platform. Lab on a Chip 16:1447-1456.

596

597

598
599
600
601
602
603
604
605

Supplemental information



624 **Table S1:** Physical properties used in finite element models of hydrogel treatments. * measured
 625 values, \ddagger default material values in COMSOL

Parameter	Symbol	Value	Unit	Reference
IRE Voltage	V_{IRE}	450	[V]	*
H-FIRE Voltage	V_{HFIRE}	450-700	[V]	*
Electrode Density	ρ_e	7850	[kg/m ³]	\ddagger
Electrode Specific Heat Capacity	Cp_e	475	[J/(kg·K)]	\ddagger
Electrode Thermal Conductivity	k_e	44.5	[W/(m·K)]	\ddagger
Electrode Conductivity	σ_e	4.03×10^6	[S/m]	\ddagger
Electrode Permittivity	ϵ_e	1		\ddagger
Hydrogel Density	ρ_h	997.8	[kg/m ³]	(45)
Hydrogel Specific Heat Capacity	Cp_h	4181.8	[J/(kg·K)]	(45)
Hydrogel Thermal Conductivity	k_h	0.6	[W/(m·K)]	(45)
Hydrogel Conductivity	σ_h	1.2	[S/m]	(45)
Hydrogel Permittivity	ϵ_h	0		(45)

626
 627
 628
 629
 630
 631
 632
 633
 634
 635
 636
 637
 638
 639
 640

641 **Table S2:** Physical properties used in finite element models of single cells. * measured values, \ddagger
 642 approximation based on water composition

Parameter	Symbol	Value	Units	Reference
Media Conductivity	σ_m	0.98	[S/m]	*
Media Permittivity	ϵ_m	$80\epsilon_0$	[F/m]	\ddagger
Cytoplasm Conductivity	σ_{cyt}	0.3	[S/m]	(46)
Cytoplasm Permittivity	ϵ_{cyt}	$154.4\epsilon_0$	[F/m]	(47)

Nucleoplasm Conductivity	σ_{nuc}	1.35	[S/m]	(46)
Nucleoplasm Permittivity	ϵ_{nuc}	$52\epsilon_0$	[F/m]	(46)
Cell Membrane Thickness	t_{mem}	5×10^{-9}	[m]	(48)
Nuclear Membrane Thickness	t_{Nmem}	40×10^{-9}	[m]	(46)
Cell Membrane Conductivity	σ_{mem}	3×10^{-7}	[S/m]	(49)
Cell Membrane Permittivity	ϵ_{mem}	$8.57\epsilon_0$	[F/m]	(50)
Nuclear Membrane Conductivity	σ_{Nmem}	6×10^{-3}	[S/m]	(46)
Nuclear Membrane Permittivity	ϵ_{Nmem}	$28\epsilon_0$	[F/m]	(46)
Domain Side Length	L_d	300×10^{-6}	[m]	-
Benign Cell Radius	R_c	20×10^{-6}	[m]	*
Benign Nuclear Radius	R_n	6.2×10^{-6}	[m]	*
Malignant Cell Radius	R_{mc}	20×10^{-6}	[m]	*
Malignant Nuclear Radius	R_{mn}	14.7×10^{-6}	[m]	*
Malignant Cell Radius (post-ephrin)	R_{mce}	16.7×10^{-6}	[m]	*
Malignant Nuclear Radius (post-ephrin)	R_{mne}	14.7×10^{-6}	[m]	*

643
644
645
646
647
648
649

650 **Supplemental Methods**

651

652 **Finite element analysis**

653 The electric field distribution within the hydrogel was found by solving the Laplace Equation:

654
$$\nabla^2 \phi = 0 \quad (\text{S-9})$$

655 where ϕ is the electrical potential. The boundaries of one electrode were set to the applied voltage
656 ($\phi = V_{\text{applied}}$) and the boundaries of the second were set to ground ($\phi = 0$) while the initial voltage
657 (V_0) for all subdomains were set to 0V. All other external boundaries were set to electrical
658 insulation ($-\mathbf{n} \cdot \mathbf{J} = 0$). The mesh was refined until error between successive refinements was less
659 than 1%. The final mesh contained 47,438 elements and solutions were found in approximately
660 3 minutes on a Pentium i3 processor.

661 In order to better understand the effect of high frequency components of H-FIRE on individual
662 cells a frequency-dependent module was used to mimic the increase in frequency for different H-
663 FIRE pulse lengths and IRE-type pulses. The geometry and physical properties of the cell can be
664 found in Supplemental Table 2.

665

666 Simulations were solved in the frequency-domain using an electric currents module. To account
667 for the impedance posed by the membranes of the cell and nucleus their boundaries were
668 assigned impedance properties found in literature (Supplemental Table 2). While some equations
669 such as the one presented by Huang *et al* have been useful for calculating the TMP for cells
670 exposed to an AC signal, further development of the model needs to be done (51). Our group
671 developed an equivalent circuit model considering the general dimensions, conductivity, and
672 permittivity of the cell membrane, cytoplasm, nucleic envelope, and nucleus. While the equation

673 describing this model can be further refined it provides evidence that changes to the NCR mostly
674 affect the capacitive component representing the cytoplasm.

675

676

677 **References**

678 1. Weaver, J. C., and Y. A. Chizmadzhev. 1996. Theory of electroporation: A review.
679 Bioelectrochemistry and Bioenergetics 41:135-160.

680 2. Mir, L. M. 2001. Therapeutic perspectives of in vivo cell electropermeabilization.
681 Bioelectrochemistry 53:1-10.

682 3. Agerholm-Larsen, B., H. K. Iversen, P. Ibsen, J. M. Moller, F. Mahmood, K. S. Jensen, and J. Gehl.
683 2011. Preclinical validation of electrochemotherapy as an effective treatment for brain tumors.
684 Cancer research 71:3753-3762.

685 4. Davalos, R. V., L. Mir, and B. Rubinsky. 2005. Tissue ablation with irreversible electroporation.
686 Annals of biomedical engineering 33:223-231.

687 5. Cannon, R., S. Ellis, D. Hayes, G. Narayanan, and R. C. Martin. 2013. Safety and early efficacy of
688 irreversible electroporation for hepatic tumors in proximity to vital structures. Journal of surgical
689 oncology 107:544-549.

690 6. Onik, G., and B. Rubinsky. 2010. Irreversible electroporation: first patient experience focal
691 therapy of prostate cancer. In *Irreversible Electroporation*. Springer. 235-247.

692 7. Martin, R. C., D. Kwon, S. Chalikonda, M. Sellers, E. Kotz, C. Scoggins, K. M. McMasters, and K.
693 Watkins. 2015. Treatment of 200 locally advanced (stage III) pancreatic adenocarcinoma
694 patients with irreversible electroporation: safety and efficacy. Annals of surgery 262:486-494.

695 8. Neal, R. E., J. L. Millar, H. Kavnoudias, P. Royce, F. Rosenfeldt, A. Pham, R. Smith, R. V. Davalos,
696 and K. R. Thomson. 2014. In vivo characterization and numerical simulation of prostate
697 properties for non-thermal irreversible electroporation ablation. The Prostate 74:458-468.

698 9. Lee, E. W., C. Chen, V. E. Prieto, S. M. Dry, C. T. Loh, and S. T. Kee. 2010. Advanced hepatic
699 ablation technique for creating complete cell death: irreversible electroporation 1. Radiology
700 255:426-433.

701 10. Guo, Y., Y. Zhang, R. Klein, G. M. Nijm, A. V. Sahakian, R. A. Omary, G.-Y. Yang, and A. C. Larson.
702 2010. Irreversible electroporation therapy in the liver: longitudinal efficacy studies in a rat
703 model of hepatocellular carcinoma. Cancer research 70:1555-1563.

704 11. Daniels, C., and B. Rubinsky. 2009. Electrical field and temperature model of nonthermal
705 irreversible electroporation in heterogeneous tissues. Journal of biomechanical engineering
706 131:071006.

707 12. Lee, E. W., C. T. Loh, and S. T. Kee. 2007. Imaging guided percutaneous irreversible
708 electroporation: ultrasound and immunohistological correlation. Technology in cancer research
709 & treatment 6:287-293.

710 13. Bonakdar, M., E. L. Latouche, R. L. Mahajan, and R. V. Davalos. 2015. The feasibility of a smart
711 surgical probe for verification of ire treatments using electrical impedance spectroscopy. Ieee T
712 Bio-Med Eng 62:2674-2684.

713 14. Neal II, R., J. Rossmeisl Jr, V. D'Alfonso, J. Robertson, P. Garcia, S. Elankumaran, and R. Davalos.
714 2014. In vitro and numerical support for combinatorial irreversible electroporation and
715 electrochemotherapy glioma treatment. Annals of biomedical engineering 42:475-487.

716 15. Wykosky, J., D. M. Gibo, C. Stanton, and W. Debinski. 2005. EphA2 as a Novel Molecular Marker
717 and Target in Glioblastoma Multiforme. Molecular Cancer Research 3:541-551.

718 16. Hatano, M., J. Eguchi, T. Tatsumi, N. Kuwashima, J. E. Dusak, M. S. Kinch, I. F. Pollack, R. L.
719 Hamilton, W. J. Storkus, and H. Okada. 2005. EphA2 as a Glioma-Associated Antigen: A Novel
720 Target for Glioma Vaccines. Neoplasia 7:717-722.

721 17. Liu, D.-P., Y. Wang, H. P. Koeffler, and D. Xie. 2007. Ephrin-A1 is a negative regulator in glioma
722 through down-reguation of EphA2 and FAK. International journal of oncology 30:865-872.

723 18. Wykosky, J., E. Palma, D. Gibo, S. Ringler, C. Turner, and W. Debinski. 2008. Soluble monomeric
724 EphrinA1 is released from tumor cells and is a functional ligand for the EphA2 receptor.
725 *Oncogene* 27:7260-7273.

726 19. Wykosky, J., D. M. Gibo, and W. Debinski. 2007. A novel, potent, and specific ephrinA1-based
727 cytotoxin against EphA2 receptor-expressing tumor cells. *Molecular cancer therapeutics* 6:3208-
728 3218.

729 20. Ferluga, S., R. Hantgan, Y. Goldgur, J. P. Himanen, D. B. Nikolov, and W. Debinski. 2013.
730 Biological and Structural Characterization of Glycosylation on Ephrin-A1, a Preferred Ligand for
731 EphA2 Receptor Tyrosine Kinase. *The Journal of Biological Chemistry* 288:18448-18457.

732 21. Miao, H., E. Burnett, M. Kinch, E. Simon, and B. Wang. 2000. Activation of EphA2 kinase
733 suppresses integrin function and causes focal-adhesion-kinase dephosphorylation. *Nature cell
734 biology* 2:62-69.

735 22. Eppich, H. M., R. Foxall, K. Gaynor, D. Dombkowski, N. Miura, T. Cheng, S. Silva-Arrieta, R. H.
736 Evans, J. A. Mangano, F. I. Preffer, and D. T. Scadden. 2000. Pulsed electric fields for selection of
737 hematopoietic cells and depletion of tumor cell contaminants. *Nat Biotech* 18:882-887.

738 23. Agarwal, A., I. Zudans, E. A. Weber, J. Olofsson, O. Orwar, and S. G. Weber. 2007. Effect of cell
739 size and shape on single-cell electroporation. *Analytical chemistry* 79:3589-3596.

740 24. Van den Bos, W., D. de Bruin, B. Muller, I. Varkarakis, A. Karagiannis, P. Zondervan, M. L. Pes, D.
741 Veelo, C. S. Heijink, and M. Engelbrecht. 2014. The safety and efficacy of irreversible
742 electroporation for the ablation of prostate cancer: a multicentre prospective human *in vivo*
743 pilot study protocol. *BMJ open* 4:e006382.

744 25. Ivey, J. W., E. L. Latouche, M. B. Sano, J. H. Rossmeisl, R. V. Davalos, and S. S. Verbridge. 2015.
745 Targeted cellular ablation based on the morphology of malignant cells. *Scientific reports* 5.

746 26. Arena, C. B., M. B. Sano, J. H. Rossmeisl, J. L. Caldwell, P. A. Garcia, M. N. Rylander, and R. V.
747 Davalos. 2011. High-frequency irreversible electroporation (H-FIRE) for non-thermal ablation
748 without muscle contraction. *Biomedical engineering online* 10:102.

749 27. Foster, K. R. 2000. Thermal and nonthermal mechanisms of interaction of radio-frequency
750 energy with biological systems. *IEEE Transactions on Plasma Science* 28:15-23.

751 28. Arena, C. B., M. B. Sano, M. N. Rylander, and R. V. Davalos. 2011. Theoretical considerations of
752 tissue electroporation with high-frequency bipolar pulses. *IEEE T Bio-Med Eng* 58:1474-1482.

753 29. Cross, V. L., Y. Zheng, N. W. Choi, S. S. Verbridge, B. A. Sutermaster, L. J. Bonassar, C. Fischbach,
754 and A. D. Stroock. 2010. Dense type I collagen matrices that support cellular remodeling and
755 microfabrication for studies of tumor angiogenesis and vasculogenesis *in vitro*. *Biomaterials*
756 31:8596-8607.

757 30. Sano, M. B., C. B. Arena, M. R. DeWitt, D. Saur, and R. V. Davalos. 2014. In-vitro bipolar nano-
758 and microsecond electro-pulse bursts for irreversible electroporation therapies.
759 *Bioelectrochemistry* 100:69-79.

760 31. Bhonsle, S. P., C. B. Arena, D. C. Sweeney, and R. V. Davalos. 2015. Mitigation of impedance
761 changes due to electroporation therapy using bursts of high-frequency bipolar pulses.
762 *Biomedical engineering online* 14:S3.

763 32. White, F., and K. Gohari. 1981. Variations in the nuclear-cytoplasmic ratio during epithelial
764 differentiation in experimental oral carcinogenesis. *Journal of Oral Pathology & Medicine*
765 10:164-172.

766 33. Jin, Y., L. Yang, and F. White. 1995. Preliminary assessment of the epithelial nuclear-cytoplasmic
767 ratio and nuclear volume density in human palatal lesions. *Journal of oral pathology & medicine*
768 24:261-265.

769 34. Boyd, A. W., P. F. Bartlett, and M. Lackmann. 2014. Therapeutic targeting of EPH receptors and
770 their ligands. *Nature reviews Drug discovery* 13:39-62.

771 35. Pasquale, E. B. 2010. Eph receptors and ephrins in cancer: bidirectional signalling and beyond.
772 *Nat Rev Cancer* 10:165-180.

773 36. Miao, H., and B. Wang. 2012. EphA receptor signaling—Complexity and emerging themes.
774 *Seminars in Cell & Developmental Biology* 23:16-25.

775 37. Zelinski, D. P., N. D. Zantek, J. C. Stewart, A. R. Irizarry, and M. S. Kinch. 2001. EphA2
776 overexpression causes tumorigenesis of mammary epithelial cells. *Cancer research* 61:2301-
777 2306.

778 38. Miyazaki, T., H. Kato, M. Fukuchi, M. Nakajima, and H. Kuwano. 2003. EphA2 overexpression
779 correlates with poor prognosis in esophageal squamous cell carcinoma. *International journal of*
780 *cancer* 103:657-663.

781 39. Thaker, P. H., M. Deavers, J. Celestino, A. Thornton, M. S. Fletcher, C. N. Landen, M. S. Kinch, P.
782 A. Kiener, and A. K. Sood. 2004. EphA2 expression is associated with aggressive features in
783 ovarian carcinoma. *Clinical Cancer Research* 10:5145-5150.

784 40. Li, X., Y. Wang, Y. Wang, Z. Haining, H. Yang, F. Zhou, J. Zhang, W. Liu, Y. Wang, and X. Zhang.
785 2007. Expression of EphA2 in Human Astrocytic Tumors: Correlation with Pathologic Grade,
786 Proliferation and Apoptosis. *Tumor Biology* 28:165-172.

787 41. Wang, L.-F., E. Fokas, M. Bieker, F. Rose, P. Rexin, Y. Zhu, A. Pagenstecher, R. Engenhart-Cabillic,
788 and H.-X. An. 2008. Increased expression of EphA2 correlates with adverse outcome in primary
789 and recurrent glioblastoma multiforme patients. *Oncology reports* 19:151-156.

790 42. Liu, F., P. J. Park, W. Lai, E. Maher, A. Chakravarti, L. Durso, X. Jiang, Y. Yu, A. Brosius, and M.
791 Thomas. 2006. A genome-wide screen reveals functional gene clusters in the cancer genome
792 and identifies EphA2 as a mitogen in glioblastoma. *Cancer research* 66:10815-10823.

793 43. Liu, G., X. Yuan, Z. Zeng, P. Tunici, H. Ng, I. R. Abdulkadir, L. Lu, D. Irvin, K. L. Black, and S. Y. John.
794 2006. Analysis of gene expression and chemoresistance of CD133+ cancer stem cells in
795 glioblastoma. *Molecular cancer* 5:67.

796 44. Binda, E., A. Vissioli, F. Giani, G. Lamorte, M. Copetti, K. L. Pitter, J. T. Huse, L. Cajola, N. Zanetti,
797 and F. DiMeco. 2012. The EphA2 receptor drives self-renewal and tumorigenicity in stem-like
798 tumor-propagating cells from human glioblastomas. *Cancer cell* 22:765-780.

799 45. Rubinsky, B. 2007. Irreversible electroporation in medicine. *Technology in cancer research &*
800 *treatment* 6:255-259.

801 46. Asami, K., Y. Takahashi, and S. Takashima. 1989. Dielectric-Properties of Mouse Lymphocytes
802 and Erythrocytes. *Biochim Biophys Acta* 1010:49-55.

803 47. Yang, J., Y. Huang, X. J. Wang, X. B. Wang, F. F. Becker, and P. R. C. Gascoyne. 1999. Dielectric
804 properties of human leukocyte subpopulations determined by electrorotation as a cell
805 separation criterion. *Biophysical Journal* 76:3307-3314.

806 48. Gascoyne, P. R. C., R. Pethig, J. P. H. Burt, and F. F. Becker. 1993. Membrane-Changes
807 Accompanying the Induced-Differentiation of Friend Murine Erythroleukemia-Cells Studied by
808 Dielectrophoresis. *Biochim Biophys Acta* 1149:119-126.

809 49. Sano, M. B., E. A. Henslee, E. M. Schmelz, and R. V. Davalos. 2011. Contactless dielectrophoretic
810 spectroscopy: Examination of the dielectric properties of cells found in blood. *Electrophoresis*
811 32:3164-3171.

812 50. Alberts, B., D. Bray, J. Lewis, M. Raff, K. Roberts, J. D. Watson, and A. Grimstone. 1995.
813 *Molecular Biology of the Cell* (3rd edn). *Trends in Biochemical Sciences* 20:210-210.

814 51. Huang, S.-H., L.-Y. Hung, and G.-B. Lee. 2016. Continuous nucleus extraction by optically-induced
815 cell lysis on a batch-type microfluidic platform. *Lab on a Chip* 16:1447-1456.

817

818

819

820